Ann. Geophys., 27, 591–600, 2009
www.ann-geophys.net/27/591/2009/

Annales Geophysicae

Superposed epoch analysis of the ionospheric convection evolution during substorms: onset latitude dependence

A. Grocott[1], **J. A. Wild**[2], **S. E. Milan**[1], **and T. K. Yeoman**[1]

[1]Department of Physics and Astronomy, University of Leicester, University Road, Leicester, LE1 7RH, UK
[2]Department of Communication Systems, InfoLab21, Lancaster University, Lancaster, LA1 4WA, UK

Received: 18 August 2008 – Revised: 6 January 2009 – Accepted: 13 January 2009 – Published: 6 February 2009

Abstract. Using data from the Super Dual Auroral Radar Network (SuperDARN) we investigate the ionospheric convection response to magnetospheric substorms. Substorms were identified using the Far Ultraviolet (FUV) instrument on board the Imager for Magnetopause-to-Aurora Global Exploration (IMAGE) spacecraft, and were then binned according to the magnetic latitude of their onset. A superposed epoch analysis of the ionospheric convection patterns for each onset-latitude bin was then performed using radar data for the interval 60 min before onset to 90 min after. It is found that lower onset-latitude substorms are associated with generally more enhanced convection than the higher latitude substorms, although they suffer from a significant localised reduction of the flow in the midnight sector during the expansion phase. Higher-latitude substorms are associated with a significant and rapid increase in the nightside convection following substorm onset, with all onset-latitude bins showing an enhancement over onset values by ∼60 min into the expansion phase. A rudimentary inspection of the concurrent auroral evolution suggests that the duration of the flow reduction following substorm onset is dependent on the strength and duration of the expansion phase aurora and its associated conductivity enhancement.

Keywords. Ionosphere (Auroral ionosphere; Plasma convection) – Magnetospheric physics (Storms and substorms)

1 Introduction

Magnetospheric substorms are understood to be one of the primary mechanisms by which the Earth's magnetotail rids itself of stored magnetic flux and energy that are accumulated through the action of reconnection with the interplanetary magnetic field. Whilst the exact time sequence of events which surrounds the onset of magnetospheric substorms is still under debate, it has recently been suggested that substorms are initiated by near-Earth reconnection in the magnetotail (Angelopoulos et al., 2008), which pinches off closed magnetic flux and then closes open magnetic flux, exciting magnetospheric convection (e.g. Baker et al., 1996). Within a few minutes a disruption of the cross-tail current is also observed in the inner magnetosphere, leading to the creation of the substorm current wedge (e.g. Lui, 1996) and an associated ionospheric auroral disturbance (Akasofu, 1964). There have been mixed reports, however, regarding the nature of the ionospheric convection that accompanies this disturbance. We address this issue in the present paper.

It was suggested by Cowley et al. (1998) that reconnection during substorms should excite large-scale twin-vortex flow in the high-latitude ionosphere. In an early study of Sondrestrom radar data, Blanchard et al. (1997) found that an increase in the tail reconnection rate occurs near midnight shortly after substorm expansion phase onset. Initially, however, this increase was mainly manifest in a poleward motion of the inferred open-closed field line boundary with the flows becoming elevated only after an interval of ∼30 min. Somewhat correspondingly, Weimer (1999) presented a statistical survey of low-altitude electric field data from the DE-2 spacecraft, separated according to the IMF direction and into substorm and non-substorm intervals. The flow patterns for a given IMF orientation showed a more pronounced "Harang" asymmetry on the nightside during substorm intervals

Correspondence to: A. Grocott
(a.grocott@ion.le.ac.uk)

Published by Copernicus Publications on behalf of the European Geosciences Union.

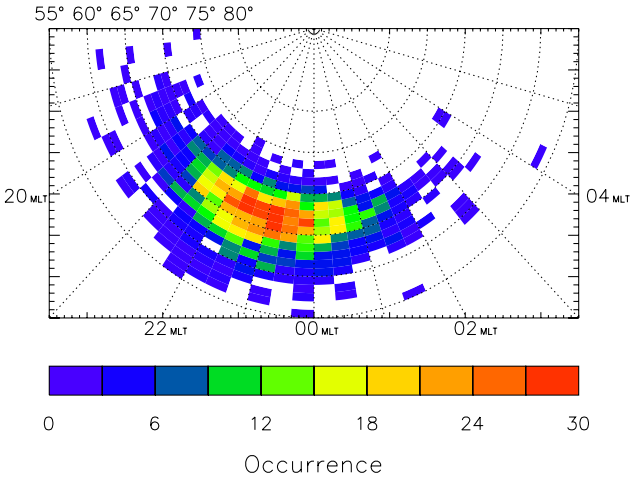

Fig. 1. The locations of Northern Hemisphere isolated substorm onsets, observed by the FUV instrument on-board the IMAGE satellite, presented in magnetic latitude – magnetic local time coordinates. The occurrence of substorms within each latitude – local time bin is colour coded according to the scale at the bottom.

than during non-substorm intervals, but the total transpolar voltage values showed little overall difference. On the other hand, Opgenoorth and Pellinen (1998) presented evidence for flow enhancements in the dusk auroral zone immediately following expansion phase onset in the midnight sector, leading to an immediate increase in the global "directly driven" current system. They suggest, however, that diversion of the twin-vortex flow around the low-flow high-conductivity auroral bulge formed during the expansion phase (e.g. Morelli et al., 1995; Yeoman et al., 2000) may play a role. More recently, Grocott et al. (2002) presented an analysis of Super Dual Auroral Radar Network (SuperDARN) flow data obtained during an isolated substorm, and found evidence for the excitation of twin-vortex flow cells centred in the nightside ionosphere, which enhance the transpolar voltage by ∼40 kV compared with pre-onset values. Further studies using SuperDARN have produced mixed results, however, by providing evidence for both the excitation (e.g. Grocott et al., 2006; Provan et al., 2004) and reduction (e.g. Lyons et al., 2001; Bristow and Jensen, 2007) of the flows following substorm onset.

Using the Frey et al. (2004) substorm database Milan et al. (2009) performed a superposed epoch analysis of the auroral evolution of substorms. They found that the auroral morphology was only reproducible in an average sense if substorms were grouped according to onset magnetic latitude, due largely to the fact that substorm intensity is intrinsically linked to the pre-existing open flux content of the polar cap. In the present paper we therefore use a similar latitude grouping to produce a set of average substorm convection patterns for each onset-latitude group. These patterns are obtained for the interval from 60 min before, to 90 min after, each of the 1979 isolated Northern Hemisphere substorms in the Frey list, using the radar data set discussed by Wild and Grocott (2008). We find that there is a clear difference in the ionospheric convection response to substorms of differing onset latitudes. Higher-latitude substorms are associated with a significant and prompt increase in the nightside convection following onset, whereas lower-latitude substorms appear to be associated with an initial decrease in the nightside flows, with a delay of up to ∼60 min before any enhancement is observed.

2 Data analysis

Using the FUV instrument (Mende et al., 2000a,b) on the IMAGE spacecraft Frey et al. (2004) identified 2437 substorms occurring between May 2000 and December 2002, subsequently extending this number to 4193 after considering the 5-year period up to December 2005. Wild and Grocott (2008) refined this list to 3005 isolated events (by excluding those known to have occurred within ±2 h of another substorm), 1979 of which were observed in the Northern Hemisphere. The onset locations of these 1979 events (see Fig. 1) have a mean magnetic latitude of 66° and a mean magnetic local time (MLT) of 23 h. For the purposes of the present study we have grouped these events into 10 magnetic latitude bins: below 61°, 61–62°..., 68–69°, and above 69°. For each event we define a "substorm epoch" as being an interval of time running from 60 min before, to 90 min after, the onset time of the substorm.

Ionospheric flow data for each substorm epoch are provided by the Super Dual Auroral Radar Network (SuperDARN). The SuperDARN network of HF radars provides almost continuous measurements of ionospheric convection velocities in the auroral regions of the Northern and Southern Hemispheres (Greenwald et al., 1995; Chisham et al., 2007) and this facilitates the routine production of large scale maps of the high-latitude convection using the "Map Potential" technique (Ruohoniemi and Baker, 1998). This technique involves the mapping of line-of-sight radar velocity measurements onto an equal area polar grid and using them to derive a best-fit solution to an nth-order expansion of the electrostatic potential, expressed in spherical harmonics. An investigation into the sensitivity of the choice of n on the results of the present study revealed that a relatively low sixth order expansion was suitable for resolving the larger-scale character of the convection pattern. A boundary defining the zero potential at the equatorward edge of the convection pattern is also determined from the radar data to help constrain the solution at lower latitudes.

Two methods of investigating the average substorm convection have been adopted for this study. The first method provides a means by which we can investigate the best-fit average large-scale convection patterns and involves using the

Map Potential "gridded" radar data files generated by Wild and Grocott (2008) to derive superposed epoch convection patterns for the ten onset-latitude bins. This is achieved by combining the gridded radar data from all of the substorm epochs in each of the ten onset-latitude bins into ten superposed substorm epochs and then performing the Map Potential fit on each one. The maximum number of substorms in any one onset-latitude bin is 305, however, owing to data processing limitations we restricted the number of substorm epochs combined in any one Map Potential fit to 150. Where an onset-latitude bin contained more than 150 substorms a random sample of 150 was used. Having performed the analysis on a number of different random samples we can confirm that little difference is evident in the large-scale nature of the patterns.

It is also necessary to manually specify the magnetic latitude of the zero-potential boundary, Λ_0, for these average convection maps. In the Map Potential analysis, this boundary is set to be the lowest latitude at which a significant number of flow vectors above a specified velocity threshold are observed. For the usual "individual-epoch" analysis this is usually set to be 3 flow vectors above 100 m s^{-1}, which is generally sufficient to exclude any noise and interference which might otherwise mislead the algorithm and force it to set the boundary too low. When adding such a large volume of radar data together however, as is the case for the superposed epoch analysis, this technique generally fails. We have therefore specified the boundary to be the mean of the boundaries identified at each time step for all of the individual substorm epochs. Whilst this might not necessarily be the best choice in each individual case, it is an objective and consistent method across all times and onset-latitude bins and makes direct comparisons between different convection patterns straightforward.

The second method we have used to investigate the average convection involves using a statistical database of ionospheric convection data to study the average nightside flows in a more localised manner. This database has been created to facilitate studies involving large volumes of SuperDARN data and consists of a reduced set of 40 velocity measurements (and associated data coverage information) for every 2 min interval between 1999 and 2006. These measurements are derived for the centre points of a set of boxes, the locations of which are fixed in magnetic local time but are scaled in magnetic latitude according to the overall size of the convection pattern, as shown in Fig. 2. In other words, the lowest latitude boxes are located just poleward of the zero-potential boundary of the convection pattern, Λ_0, (the green curve in Fig. 2), with a further three sets of boxes at latitudes evenly distributed between the first set and the pole. By fixing the latitude of these boxes relative to Λ_0, similar statistical points correspond to the same region of the convection pattern in each case rather than simply the same magnetic latitude/local time. The boxes themselves delimit the area in which "local" data coverage is defined. In the present study we have

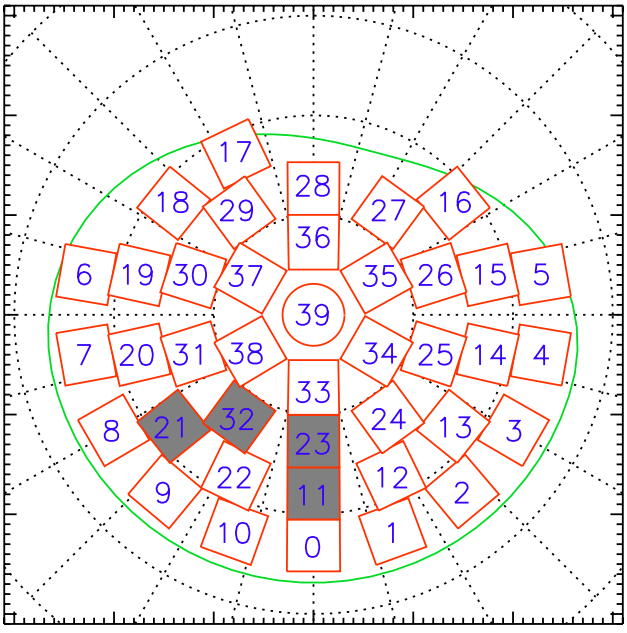

Fig. 2. The locations of the statistical data points used in the reduced SuperDARN database, plotted on a polar grid in magnetic local time – magnetic latitude coordinates with noon to the top and dusk to the left. The data points are located at the centre of the red boxes which themselves delimit the area in which local data coverage is defined. The latitudes of the boxes is shown on an arbitrary scale, being dependent on the location of the zero potential boundary, Λ_0, (shown in green) in each case. Data from the shaded boxes are discusses in the text.

imposed a condition that there must be at least 2 radar data points in a box for the corresponding velocity value to be used. This does mean that the number of events contributing to the velocity averages is not the same for each time step (overall it results in between 30% and 50% of the substorms being included in the averaging for each onset-latitude bin) but it ensures that the velocity averages from each substorm correspond to regions of the convection patterns where radar data were present to constrain the fitting. In Sect. 3.2 we present data from the boxes which are shaded in Fig. 2.

3 Observations

3.1 Large-scale convection

Examples of the average ionospheric convection (derived using the first method described in Sect. 2) surrounding substorm onset are presented in Fig. 3 which shows two sets of average superposed-epoch Northern Hemisphere patterns. In column (i) we show data from the 61°–62° onset-latitude bin and in column (ii) we show data from the 68°–69° bin. Six epoch-times are shown in each case: (a) 20 min before onset, (b) 10 min before onset, (c) at onset, (d) 8 min after onset, (e)

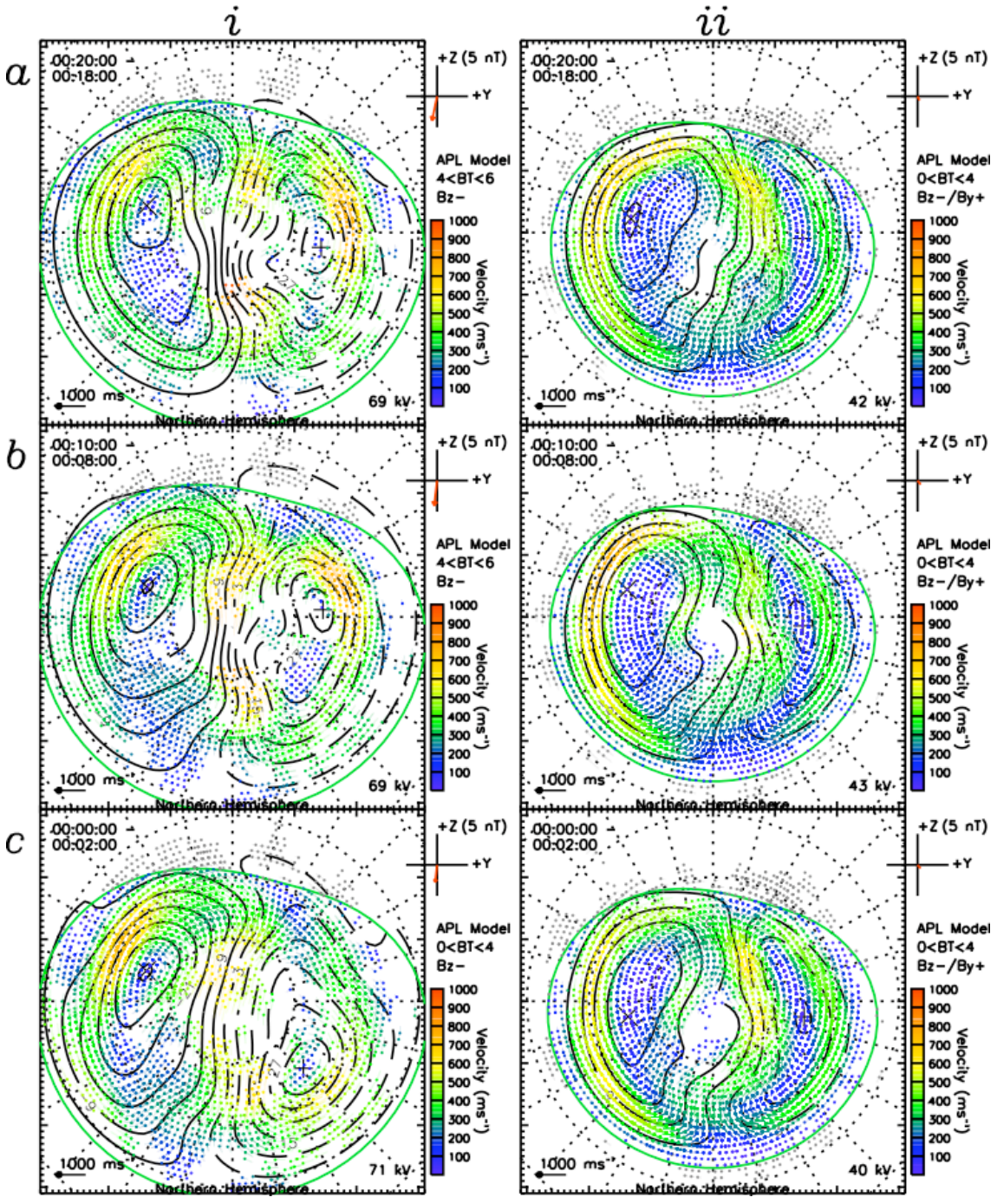

Fig. 3. Average convection patterns for the (i) 61°–62°, (ii) 68°–69° onset-latitude bins at selected times surrounding substorm onset, presented in magnetic latitude – magnetic local time coordinates with noon to the top and dusk to the left. The equipotential contours represent the plasma streamlines of the fitted convection pattern, with vectors showing the fitted velocity at the locations of the radar measurements. The velocity vectors are colour coded according to the scale shown along side each panel.

20 min after onset and (f) 50 min after onset. These convection patterns are presented in magnetic latitude – magnetic local time coordinates from 60° latitude to the pole, with noon to the top and dusk to the left. In each case, the equipotential contours represent the plasma streamlines of the fitted convection pattern, with vectors showing the fitted velocity at the locations of actual radar measurements input to the analysis. The velocity vectors are colour coded according to the

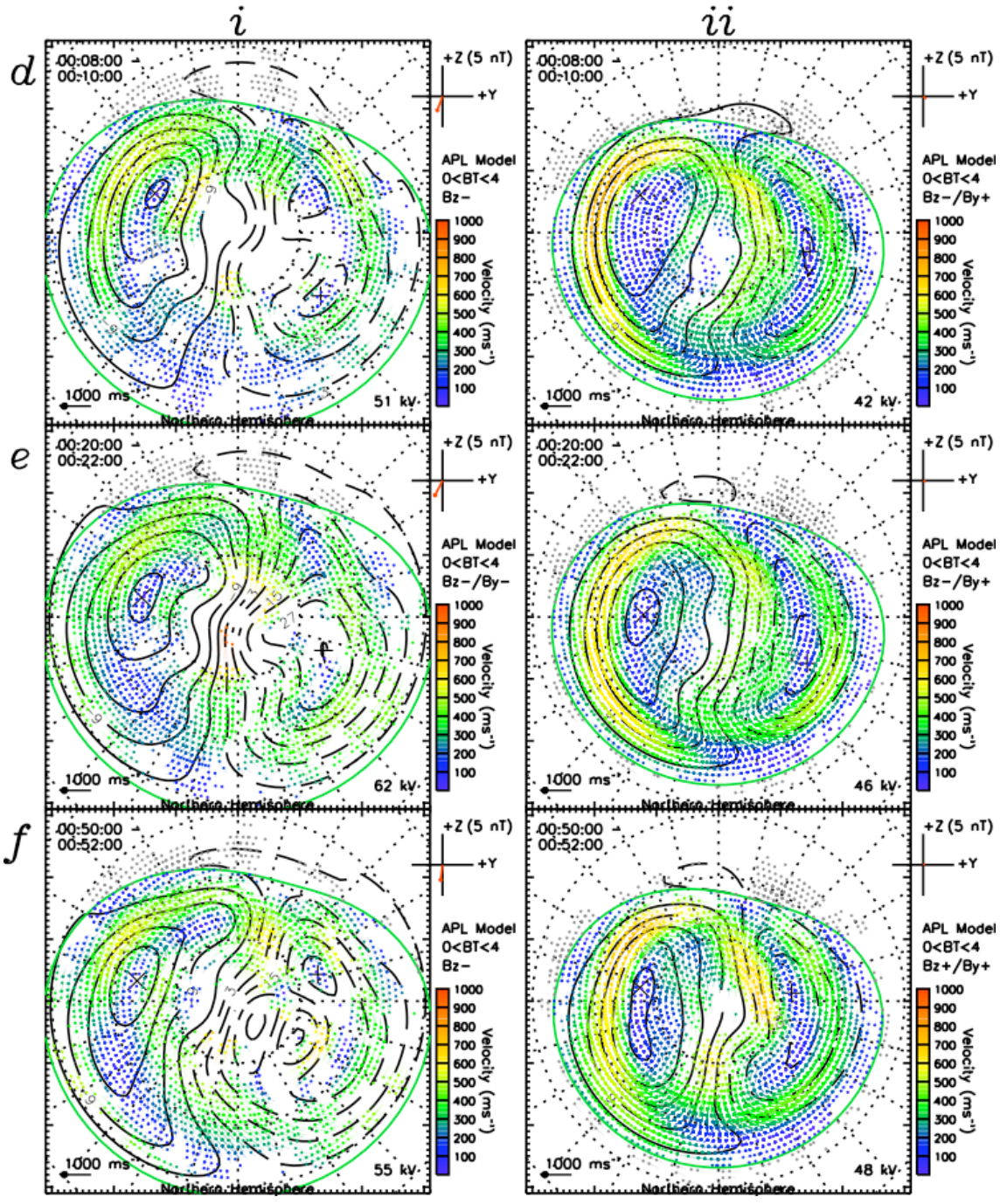

Fig. 3. Continued.

scale shown along the side of each panel. Also shown, in the bottom right hand corner of each panel, is the total transpolar voltage, V_{PC}, which provides an indication of the overall strength of the convection pattern.

The data presented in Fig. 3 reveal a number of features: the lower onset-latitude substorms (i) are associated with generally more enhanced convection than the higher latitude substorms (ii) as evidenced by both the larger size of the convection patterns and the higher values of V_{PC}. The more intense large-scale flows during the growth phase for the low-latitude substorms (i, a–b), are presumably due to a higher rate of dayside reconnection adding open flux to the magnetosphere in this case, as shown by Milan et al. (2009). At the time of substorm onset (c) some modest localised flow

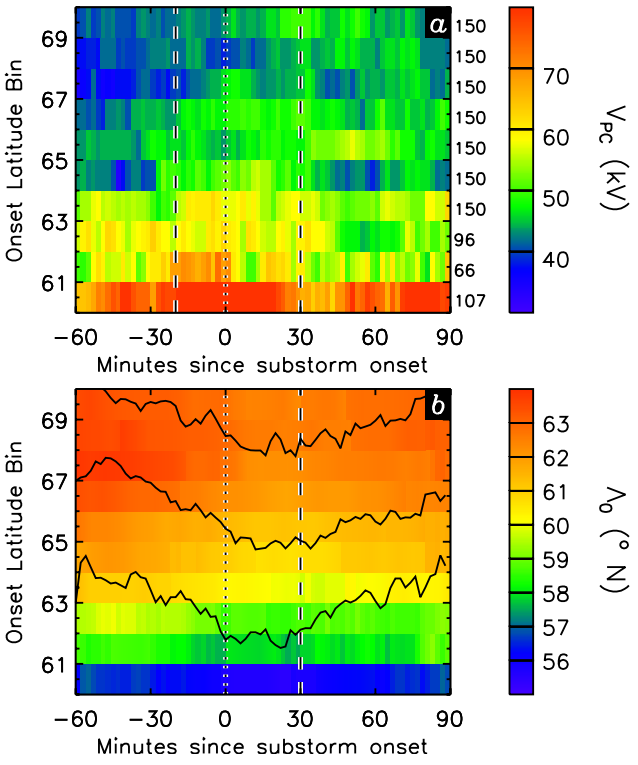

Fig. 4. **(a)** The ionospheric transpolar voltage, V_{PC} and **(b)** the magnetic latitude of the zero-potential boundary of the convection pattern, Λ_0, derived from the results of the Map Potential analysis and plotted as a function of time relative to substorm onset for the ten onset-latitude bins. In each case the parameter's magnitude is indicated by the corresponding colour bar. The vertical dotted lines indicate the time of substorm onset in the superposed-epoch and the dashed lines highlight times which are referred to in the text. On the right-hand side of panel (a) the number of substorms that contributed to the global convection analysis for each onset-latitude bin is shown.

enhancements are evident in the midnight sector at ∼70° for both onset-latitude bins, although globally there is little appreciable change, as indicated by V_{PC}. A few minutes later, however, a significant reduction of the nightside flows is readily apparent at this location for the low-latitude substorms (i,d). By comparison, (ii,d) reveals a modest enhancement in the convection over pre-onset levels for the higher-latitude substorms. By 20 min into the substorm expansion phase (e) the midnight-sector flows associated with the lower-latitude substorms have recovered somewhat (i,e), although V_{PC} is still less than that during the growth phase (62 kV vs. 69 kV). The value of V_{PC} associated with the higher-latitude substorms (ii,e) also shows a modest increase (to 46 kV), as do the nightside flows at ∼70°. These trends continue through the expansion phase to 50 min after onset (f) by which time V_{PC} has decreased further for the lower onset-latitude bin and increased for the higher-latitude bin. Locally, the midnight-sector flows still appear strong for both onset-latitude bins.

The results described above show that the ionospheric flows change in response to the substorm cycle. Whilst the evolution of the flows appears to be quite complex it is quite apparent that a difference exists between substorms of different onset latitude. To study their time-evolution more easily, Fig. 4 presents an overview of (a) the transpolar voltage, V_{PC}, and (b) the magnetic latitude of the zero-potential boundary, Λ_0, derived from the superposed-epoch convection patterns. In each case, data from the ten onset-latitude bins (vertical axis) are plotted versus substorm epoch-time, relative to substorm onset (vertical dotted line). The number of substorms that contributed to the global convection analysis for each onset-latitude bin is shown on the right-hand side of panel (a) (where 150 was an imposed maximum, as described in Sect. 2). It is clear from (a) that in general the convection becomes enhanced by ∼20 kV, ∼20 min prior to substorm onset (first vertical dashed line). For the higher-latitude substorms (onset-latitudes above ∼65°) this enhancement persists throughout the expansion phase with little evidence of any subsequent reduction. For the lower-latitude substorms (onset-latitudes below ∼65°) there is some evidence of a reduction after ∼30 min (second vertical dashed line) to pre-growth phase levels. There is also some evidence of a discontinuity between the voltage values in the lowest two onset-latitude bins. This is likely to be a result of the lowest bin containing substorms that initiated at latitudes lower than 60°. Later on in the expansion/recovery phase a number of smaller enhancements appear to occur, which could be associated with further reconnection events such as poleward boundary intensifications which are known to occur during the substorm recovery phase (Lyons et al., 1998). Overall, however, there is no clear pattern to the evolution of V_{PC} during the expansion phase beyond ∼30 min.

In panel (b) the average latitude, Λ_0, of the zero-potential boundary of the convection patterns is shown for each onset-latitude bin, to give an indication of the variation in the size of the polar cap. In addition, curves are superposed to more clearly illustrate the (relative) variation in boundary-latitude for 3 selected onset-latitude bins: under 60° (lower), 64°–65° (middle), and over 69° (upper). The scale for these curves is such that 1° on the vertical axis corresponds to a 2° change in boundary-latitude. The relationship between polar cap size and onset latitude that is implied by the variation in Λ_0 is very pronounced, with approximately 5° variation (blues through to oranges) over the 10° of the different onset-latitude bins. The variation in convection pattern size over the 90 min of the superposed-epochs is much less (of the order of 2°), but still clearly shows an expansion of the convection pattern during the growth and early expansion phases, followed by a contraction of the pattern during the late expansion and recovery phases. These are the variations that are predicted by the expanding-contracting polar cap (ECPC) paradigm, which explains how variable rates of dayside and

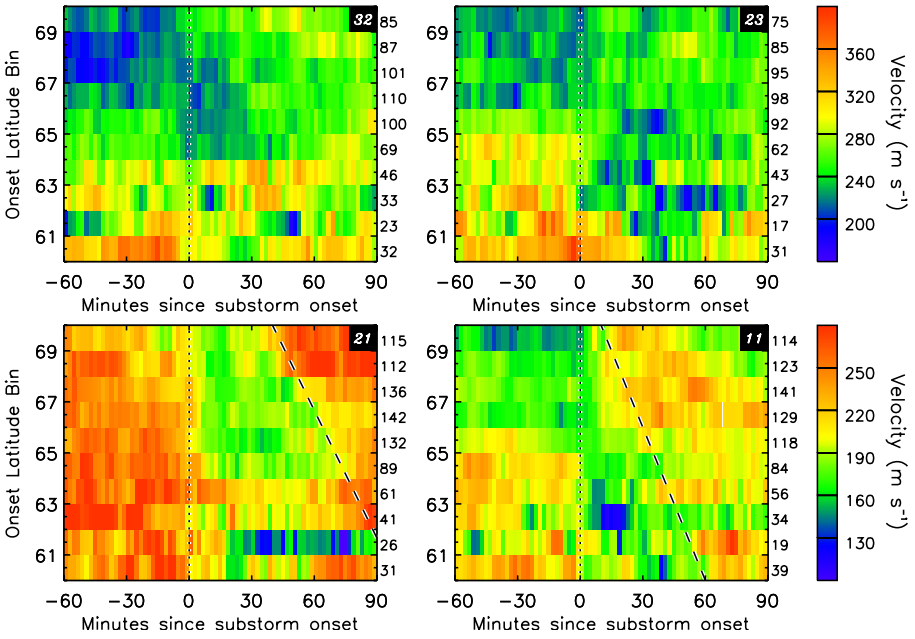

Fig. 5. Nightside ionospheric flow speeds derived from the results of the Map Potential analysis, plotted as a function of time relative to substorm onset for the ten onset-latitude bins. The locations of the flow measurements are indicated by the numbers in the upper right-hand corner of each panel, which are defined in Fig. 2. On the right-hand side of each panel, the mean number of substorms that contributed to the statistics for each onset-latitude bin is shown. The flow magnitudes are indicated by the colour bars on the right-hand side of the figure, with panels common to a row sharing the same scale. The vertical dotted lines indicate the time of substorm onset in the superposed-epoch; the dashed lines are described in the text.

nightside reconnection lead to changes in the size of the polar cap and excite magnetospheric and ionospheric convection (Cowley and Lockwood, 1992). Figure 4b therefore illustrates that dayside reconnection dominates during the substorm growth phase, resulting in the expansion of the polar cap, but that during the substorm expansion phase it is nightside reconnection which dominates, resulting in a net closure of open flux and the observed decrease in size of the polar cap.

This concept provides a possible explanation for the lack of any significant change in V_{PC} during the expansion phase, discussed above. V_{PC} is determined by both the dayside and nightside reconnection rates such that, for example, if an interval dominated by dayside reconnection driven flows was followed by an interval dominated by nightside reconnection driven flows, there is no requirement for V_{PC} to change. Spikes in the reconnection rates, such as those which might be produced by variable reconnection as suggested above, will be manifest in V_{PC}, but a change of dominance from dayside to nightside reconnection will not. It is perhaps more helpful, therefore, to look locally at the flows on the nightside which might be more directly related to nightside reconnection.

3.2 Small-scale flows

Figure 5 presents flow data obtained from the statistical convection database described in Sect. 2, from four of the box locations shown in Fig. 2 (32, 23, 21, and 11). These were chosen because they encompass the bulk of the substorm onset locations, as can be seen by comparison with Fig. 1. The magnitude of the average flow measurements for each of the ten onset-latitude bins is presented, in a similar format to Fig. 4. Again, the vertical dotted line on each panel indicates the time of substorm onset; the dashed lines are discussed below. Additionally, on the right-hand side of each panel, the mean number of substorms that contributed to the statistics for each onset-latitude bin is shown. As discussed in Sect. 2 this number is not constant over the 150 min of the superposed-epoch, however, an inspection of the variation suggests little deviation from this mean. The advantage of allowing this number to vary is that the flow averages presented are derived only from intervals where radar data were present at the location of the box. As will be discussed below, these localised flow measurements appear to exhibit more variability than the transpolar voltage over the evolution of the substorm, as well as reinforcing the onset-latitude dependence which was previously noted.

Consider the top-left panel, which shows flow data from statistical box 32. Approximately 20 min prior to substorm

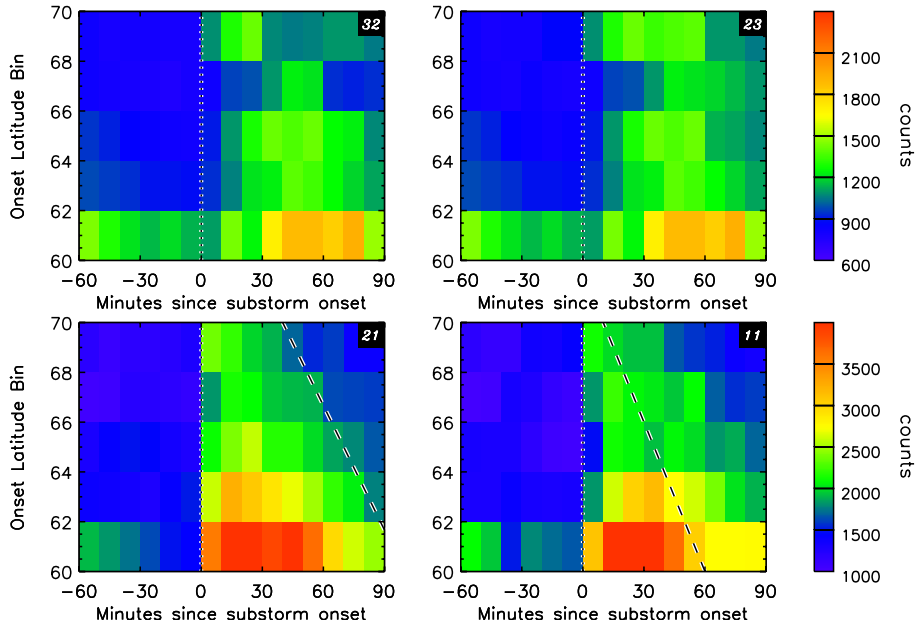

Fig. 6. 10-min averages of WIC auroral electron counts, plotted for the same locations as the flow data in Fig. 5 as a function of time relative to substorm onset, for five onset-latitude bins. The dotted and dashed lines are as in Fig. 5 (after Milan et al., 2009).

onset an enhancement can be seen in the flows, most obvious in the highest four and lowest two onset-latitude bins, which is similar to the growth phase enhancement of V_{PC} seen in Fig. 4. Around the time of onset, further changes are evident in the data. For onset-latitudes above 68° there is an enhancement in the flows from ∼200 m s^{-1} to ∼250 m s^{-1}, whereas below 67° there is a reduction of about the same magnitude. The duration of this reduction, however, appears to be related to the onset-latitude, with a subsequent enhancement occurring ∼15 min after onset for the 67°–68° bin, but not for a further ∼15 min for the 62°–63° bin. This is suggestive of a relationship between the onset-latitude and the duration of the post-onset flow reduction, discussed further below.

A similar but somewhat less clear pattern can be seen in the data from statistical box 23 (top-right), although any relationship in this case is not as obvious. The data from both of the lower-latitude statistical boxes (21 and 11, bottom panels), however, clearly reinforce the idea of a relationship between onset-latitude and the duration of a flow reduction during the early substorm expansion phase. In both cases this relationship appears to be linear, as indicated by the dashed diagonal lines. Consider first the data from magnetic local midnight (box 11). For the lowest onset-latitude bins the growth phase flows of up to 300 m s^{-1} are reduced dramatically at substorm onset, dropping to under 100 m s^{-1} by 10 to 20 min into the expansion phase. For higher onset-latitudes (above 66°), however, the magnitude of the growth phase flows is less. In this case, rather than decreasing at onset, the flows exhibit little immediate change but then proceed to increase from ∼150 m s^{-1} to ∼250 m s^{-1} after ∼10 min. Looking again at the lower onset-latitude bins, this post-onset flow enhancement can also be seen to occur, but after a delay which appears to be approximately inversely proportional to the latitude of the onset (∼5 min per degree, as indicated by the dashed slope). For the lowest onset-latitude bin this enhancement is therefore not evident until ∼60 min after onset. Finally, turning to the data in box 21 (a location ∼1.5 h west of box 11), a similar pattern is evident in the flows. Here the delay is somewhat more prolonged, certainly for higher onset-latitudes where it is ∼30 min longer, although for onset-latitudes below ∼64° there is some evidence of a threshold to this delay of ∼60–70 min where this linear relationship breaks down.

3.3 Substorm auroral evolution

As discussed in Sect. 1, it has previously been suggested that the ionospheric convection during substorms is related to the associated auroral development. In this section we therefore briefly consider the auroral development as a possible explanation for the delayed convection response described above. In Fig. 6 we show data based on the work of Milan et al. (2009) that was derived from a subset of the Frey et al. (2004) list of substorms, similar to the subset used in the present study. Auroral electron counts from the Wideband Imaging Camera (WIC) on the IMAGE spacecraft are presented as a function of substorm epoch-time, for a range of onset latitudes, for the same set of locations discussed in Fig. 5. The onset time is again marked with the vertical dotted line

in each panel, and the dashed lines from Fig. 5 are also reproduced for comparison. The bottom two panels clearly illustrate that there is a strong dependence of substorm auroral intensity on onset latitude, with the lowest onset-latitude substorms having the brightest expansion phase aurora. It is also evident that the lowest onset-latitude substorms have the longest duration expansion phase, with the time taken for the initial peak in intensity to return to some lower threshold being dependent on the onset-latitude. The dashed lines from Fig. 5 are therefore quite well correlated with the auroral intensity drop, suggesting a relationship between the duration of the auroral brightening and the duration of the flow reduction. The upper two panels, being representative of the auroral intensity more poleward of the main auroral bulge, reveal an initial delay, after onset, before the peak count is observed. This is presumably indicative of the finite propagation time of the poleward expansion of the auroral bulge. The peak auroral intensities at these more poleward locations are also lower, which could explain why there was a less obvious pattern to the evolution of the flows at these higher latitudes. Overall, these results then demonstrate that, in an average sense, the flow stagnation associated with substorms depends on the strength and duration of the expansion phase aurora and associated conductivity enhancement.

4 Summary

The results discussed above reaffirm the fact that magnetospheric substorms have a measurable influence on ionospheric convection. Furthermore they show for the first time that substorms with different onset latitudes have strikingly different convection characteristics. Low onset-latitude substorms, below $\sim$64°, are generally of larger intensity and are associated with intervals of stronger convection, but more noticeably appear to result in a reduction of the flow immediately after onset. This reduction is usually attributed to enhanced conductivities in the midnight sector which dominate during large substorms and are associated with higher levels of auroral activity (Morelli et al., 1995; Yeoman et al., 2000; Milan et al., 2009). Mid-latitude substorms, between $\sim$64° and $\sim$66°, are less noticeably associated with a large-scale reduction in convection, but equally, do not produce such an immediate and remarkable enhancement in the nightside flows. High-latitude substorms, above $\sim$66°, are associated with the smallest, but most persistent, large-scale convection response to substorms, and produce the most immediate enhancement to the flow in the locally disturbed region. This suggests that higher onset-latitude substorms, during which there is a relatively low auroral conductivity enhancement, are dominated by the local electric field, whereas lower onset-latitude substorms are dominated by high conductivities which result in a suppression of the convection electric field, and consequently, the ionospheric flows. In addition to the onset-latitude dependence of the convection reported here, one would also expect there to be an observable onset-MLT dependence. This would introduce further complexity to the nature of the convection which is not revealed by the present study. Further work, currently in progress, will investigate the MLT dependence as well as any relationship to the effects of the B_Y-component of the interplanetary magnetic field.

Acknowledgements. We would like to thank the PIs of the SuperDARN radars for provision of the radar data and R. J. Barnes of the Johns Hopkins University for the "Map-Potential" algorithm. AG was supported during this study by STFC grant PP/E000983/1. SuperDARN operations at the University of Leicester are supported by STFC grant PP/E007929/1.

Topical Editor R. Nakamura thanks two anonymous referees for thier help in evaluating this paper.

References

Akasofu, S.-I.: The development of the auroral substorm, Planet. Space Sci., 12, 273–282, 1964.

Angelopoulos, V., McFadden, J. P., Larson, D., Carlson, C. W., Mende, S. B., Frey, H., Phan, T., Sibeck, D. G., Glassmeier, K.-H., Auster, U., Donovan, E., Mann, I. R., Rae, I. J., Russell, C. T., Runov, A., Zhou, X.-Z., and Kepko, L.: Tail Reconnection Triggering Substorm Onset, Science, 321, 931–935, doi:10.1126/science.1160495, 2008.

Baker, D. N., Pulkkinen, T. I., Angelopoulos, V., Baumjohann, W., and McPherron, R. L.: Neutral line model of substorms: Past results and present view, J. Geophys. Res., 101, 12975–13010, doi:10.1029/95JA03753, 1996.

Blanchard, G. T., Lyons, L. R., and de la Beaujardière, O.: Magnetotail reconnection rate during magnetospheric substorms, J. Geophys. Res., 102, 24303–24312, doi:10.1029/97JA02163, 1997.

Bristow, W. A. and Jensen, P.: A superposed epoch study of SuperDARN convection observations during substorms, J. Geophys. Res., 112, A06232, doi:10.1029/2006JA012049, 2007.

Chisham, G., Lester, M., Milan, S. E., Freeman, M. P., Bristow, W. A., Grocott, A., McWilliams, K. A., Ruohoniemi, J. M., Yeoman, T. K., Dyson, P. L., Greenwald, R. A., Kikuchi, T., Pinnock, M., Rash, J. P. S., Sato, N., Sofko, G. J., Villain, J.-P., and Walker, A. D. M.: A decade of the Super Dual Auroral Radar Network (SuperDARN): scientific achievements, new techniques and future directions, Surv. Geophys., 28, 33–109, doi:10.1007/s10712-007-9017-8, 2007.

Cowley, S. W. H. and Lockwood, M.: Excitation and decay of solar wind-driven flows in the magnetosphere-ionosphere system, Ann. Geophys., 10, 103–115, 1992.

Cowley, S. W. H., Khan, H., and Stockton-Chalk, A.: Plasma Flow in the Coupled Magnetosphere-Ionosphere System and Its Relationship to the Substorm Cycle, in: Substorms-4, edited by: Kokubun, S. and Kamide, Y., vol. 238 of Astrophysics and Space Science Library, pp. 623–628, 1998.

Frey, H. U., Mende, S. B., Angelopoulos, V., and Donovan, E. F.: Substorm onset observations by IMAGE-FUV, J. Geophys. Res., 109, A10304, doi:10.1029/2004JA010607, 2004.

Greenwald, R. A., Baker, K. B., Dudeney, J. R., Pinnock, M., Jones, T. B., Thomas, E. C., Villain, J.-P., Cerisier, J.-C., Se-

nior, C., Hanuise, C., Hunsucker, R. D., Sofko, G., Koehler, J., Nielsen, E., Pellinen, R., Walker, A. D. M., Sato, N., and Yamagishi, H.: Darn/Superdarn: A Global View of the Dynamics of High-Lattitude Convection, Space Sci. Rev., 71, 761–796, doi: 10.1007/BF00751350, 1995.

Grocott, A., Cowley, S. W. H., Sigwarth, J. B., Watermann, J. F., and Yeoman, T. K.: Excitation of twin-vortex flow in the nightside high-latitude ionosphere during an isolated substorm, Ann. Geophys., 20, 1577–1601, 2002, http://www.ann-geophys.net/20/1577/2002/.

Grocott, A., Lester, M., Parkinson, M. L., Yeoman, T. K., Dyson, P. L., Devlin, J. C., and Frey, H. U.: Towards a synthesis of substorm electrodynamics: HF radar and auroral observations, Ann. Geophys., 24, 3365–3381, 2006, http://www.ann-geophys.net/24/3365/2006/.

Lui, A. T. Y.: Current disruption in the Earth's magnetosphere: Observations and models, J. Geophys. Res., 101, 13067–13088, doi: 10.1029/96JA00079, 1996.

Lyons, L. R., Blanchard, G. T., Samson, J. C., Rouhoniemi, J. M., Greenwald, R. A., Reeves, G. D., and Scudder, J. D.: Near Earth Plasma Sheet Penetration and Geomagnetic Disturbances, in: New Perspectives on the Earth's Magnetotail, edited by Nishida, A., Baker, D. N., and Cowley, S. W. H., p. 241, 1998.

Lyons, L. R., Ruohoniemi, J. M., and Lu, G.: Substorm-associated changes in large-scale convection during the November 24, 1996 Geospace Environment Modeling event, J. Geophys. Res., 106, 397–406, doi:10.1029/1999JA000602, 2001.

Mende, S. B., Heetderks, H., Frey, H. U., Lampton, M., Geller, S. P., Abiad, R., Siegmund, O. H. W., Tremsin, A. S., Spann, J., Dougani, H., Fuselier, S. A., Magoncelli, A. L., Bumala, M. B., Murphree, S., and Trondsen, T.: Far ultraviolet imaging from the IMAGE spacecraft. 2. Wideband FUV imaging, Space Sci. Rev., 91, 271–285, 2000a.

Mende, S. B., Heetderks, H., Frey, H. U., Lampton, M., Geller, S. P., Habraken, S., Renotte, E., Jamar, C., Rochus, P., Spann, J., Fuselier, S. A., Gerard, J.-C., Gladstone, R., Murphree, S., and Cogger, L.: Far ultraviolet imaging from the IMAGE spacecraft. 1. System design, Space Sci. Rev., 91, 243–270, 2000b.

Milan, S. E., Grocott, A., Forsyth, C., Imber, S. M., Boakes, P. D., and Hubert, B.: A superposed epoch analysis of auroral evolution during substorm growth, onset and recovery: open magnetic flux control of substorm intensity, Ann. Geophys., in press, 2009.

Morelli, J. P., Bunting, R. J., Cowley, S. W. H., Farrugia, C. J., Freeman, M. P., Friis-Christensen, E., Jones, G. O. L., Lester, M., Lewis, R. V., Lühr, H., Orr, D., Pinnock, M., Reeves, G. D., Williams, P. J. S., and Yeoman, T. K.: Radar observations of auroral zone flows during a multiple-onset substorm, Ann. Geophys., 13, 1144–1163, 1995, http://www.ann-geophys.net/13/1144/1995/.

Opgenoorth, H. J. and Pellinen, R. J.: The Reaction of the Global Convection Electrojets to the Onset and Expansion of the Substorm Current Wedge, in: Substorms-4, edited by: Kokubun, S. and Kamide, Y., vol. 238 of Astrophysics and Space Science Library, pp. 663–668, 1998.

Provan, G., Lester, M., Mende, S. B., and Milan, S. E.: Statistical study of high-latitude plasma flow during magnetospheric substorms, Ann. Geophys., 22, 3607–3624, 2004, http://www.ann-geophys.net/22/3607/2004/.

Ruohoniemi, J. M. and Baker, K. B.: Large-scale imaging of high-latitude convection with Super Dual Auroral Radar Network HF radar observations, J. Geophys. Res., 103, 20797–20811, doi: 10.1029/98JA01288, 1998.

Weimer, D. R.: Substorm influence on the ionospheric electric potentials and currents, J. Geophys. Res., 104, 185–198, doi: 10.1029/1998JA900075, 1999.

Wild, J. A. and Grocott, A.: The influence of magnetospheric substorms on SuperDARN radar backscatter, J. Geophys. Res., 113, A04308, doi:10.1029/2007JA012910, 2008.

Yeoman, T. K., Davies, J. A., Wade, N. M., Provan, G., and Milan, S. E.: Combined CUTLASS, EISCAT and ESR observations of ionospheric plasma flows at the onset of an isolated substorm, Ann. Geophys., 18, 1073–1087, 2000, http://www.ann-geophys.net/18/1073/2000/.